Recent results from SND detector at VEPP-2000 collider. Measurement of pion formfactor.

Kupich Andrey

Budker Institute of Nuclear Physics,
Novosibirsk State University

on behalf of the SND collaboration

Tau and QCD physics at present and future electron-positron colliders.
December 16th-18th 2019
BINP, Novosibirsk

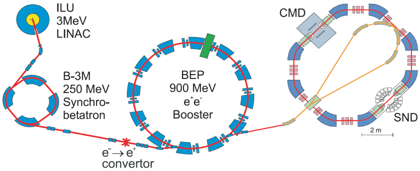

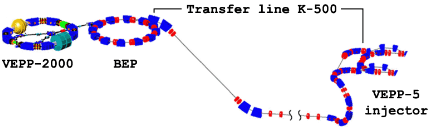

VEPP-2000 parameters

- c.m. energy E=0.3-2.0 GeV
- Luminosity at E=1.8 GeV
  $10^{32} cm^{-2} sec^{-1}$ (project)
  $4x10^{31} cm^{-2} sec^{-1}$ (achieved)
- Beam energy spread - 0.6 MeV at E=1.8 GeV

- 10 times more intense positron source
- Experiments at upgraded VEPP-2000 was restarted by the end of 2016

SND data

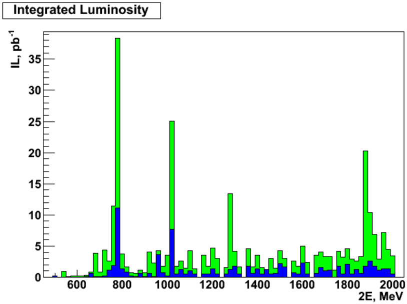

Timeline

2010-2013 – experiments, 70 pb^{-1}
2013-2016 – upgrade, new injector
2016 - ...– experiments, 210 pb^{-1}

15 hadronic processes are currently under analysis

- $e^+e^- \to \eta\pi^0\gamma$
- $e^+e^- \to \pi^+\pi^-\pi^0\eta$
- $e^+e^- \to n\bar{n}$
- $\mathbf{e^+e^- \to \pi^+\pi^-}$
- $e^+e^- \to f_1(1285)$
- $e^+e^- \to \eta$

SND detector

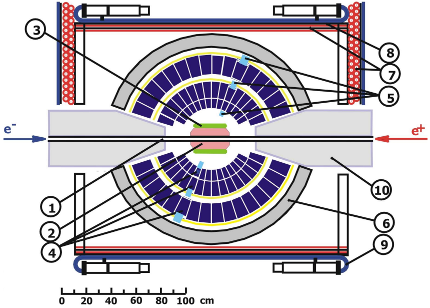

1-beam pipe, **2**-tracking system, **3**-aerogel Cherenkov counter , **4** - NaI(TI) crystals, **5** - phototriodes, **6** - iron muon absorber, **7-9** - muon detector, **10** - focusing solenoids.

Main physics task of SND is study of all possible processes of e^+e^- annihilation into hadrons below 2 GeV.

- The total hadronic cross section, which is calculated as a sum of exclusive cross sections.
- Study of hadronization (dynamics of exclusive processes).

Analysis is based on the **4.6 pb^{-1}** statistics, collected in 2012 – 2013, that corresponds to the $\mathbf{2.3 \times 10^6}$ collinear events, with $\mathbf{10^6}$ $e^+e^- \to \pi^+\pi^-, \mu^+\mu^-$ and $\mathbf{1.3 \times 10^6}$ $e^+e^- \to e^+e^-$

Events selection

1. $N_{ch} \geq 2$. The events can contain neutral particles due to nuclear interactions of charged pions with detector material or due to electromagnetic showers splitting
2. $|\Delta\theta| = |180^\circ - (\theta_1 + \theta_2)| < 12^\circ$ and $|\Delta\phi| = |180^\circ - |\phi_1 - \phi_2|| < 4^\circ$, where ϕ is the particle azimuthal angle
3. $E_{1,2} > 40$ MeV, where E_i is the ith particle $(i = 1, 2)$ energy deposition
4. $50^\circ < \theta_0 = (\theta_1 - \theta_2 + 180^\circ) \times 0.5 < 130^\circ$
5. $|d0_1| < 1$ cm , $|d0_2| < 1$ cm, where $|d0_i|$ is a distance between the ith particle track and the beam axis
6. $|z0_1| < 8$ cm , $|z0_2| < 8$ cm, where $|z0_i|$ is a distance from the center of the detector to the primary vertex of the ith particle track along the beam axis
7. The muon system $veto = 0$

The output signal of the trained BDT network R is a value in the interval from -1.0 to 1.0

The $e^+e^- \to e^+e^-$ events are located in the region $R < 0$, while $e^+e^- \to \pi^+\pi^-, \mu^+\mu^-$ events in $R > 0$.

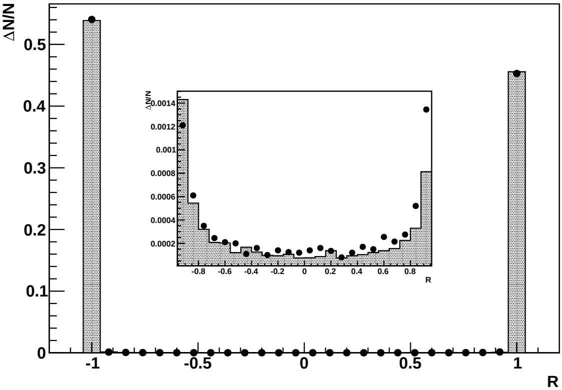

Non-collinear and cosmic backgrounds

$$N_{cosm} = N_{exp}[veto = 1] \times \frac{N_{cosm}[veto = 0]}{N_{cosm}[veto = 1]}$$

$N_{exp}[veto = 1]$ – number of data events selected with 2π cuts but with veto=1; $N_{cosm}[veto = 0(1)]$ – number of special cosmic events

Two types of cosmic events are used:

- Non-central ($|d0_1| > 0.5$ cm , $|d0_2| > 0.5$ cm, $|z0_1| > 5$ cm and $|z0_2| > 5$ cm) events from the same data sample.
- Events from special cosmic runs without beams

Both give the **same 2.5%** ratio between $N_{cosm}[veto = 0]$ and $N_{cosm}[veto = 1]$ in the **whole energy spectrum**

Non-collinear and cosmic backgrounds

Background from the $e^+e^- \to \pi^+\pi^-\pi^0$ is subtracted directly in the $\omega(782)$ region, with a number of background events estimated according to the formula:

$$N_{3\pi} = N^{exp}[3\pi] \times \frac{N^{mc}_{3\pi}[2\pi]}{N^{mc}_{3\pi}[3\pi]}$$

$N^{exp}[3\pi]$ – number of $e^+e^- \to \pi^+\pi^-\pi^0$ events in the same data sample selected with a special 3π cuts:

$$N_{cha} \geq 2,\ N_n \geq 2,\ |\Delta\theta| > 10^\circ,\ |\Delta\phi| > 10^\circ,$$
$$40^\circ < \theta_i < 140^\circ, \chi^2_{\pi^+\pi^-2\gamma} < 50,\ \chi^2_{\pi^+\pi^-\pi^0} < 30$$

Contribution of this background to the total $e^+e^- \to \pi^+\pi^-$ cross section **is less than 0.15%**, due to the strong suppression by $|\Delta\theta|$ and $|\Delta\phi|$ cuts.

ID efficiency

$$\varepsilon_e = \frac{N^{ee}(R \in [-1;0])}{N^{ee}(R \in [-1;1])}, \quad \varepsilon_\pi = \frac{N^{\pi\pi}(R \in [0;1])}{N^{\pi\pi}(R \in [-1;1])}$$

$N^{ee,\pi\pi}(R \in [a;b])$ are the numbers of $e^+e^- \to e^+e^-$ or $\pi^+\pi^-$ events with R in the interval $[a;b]$

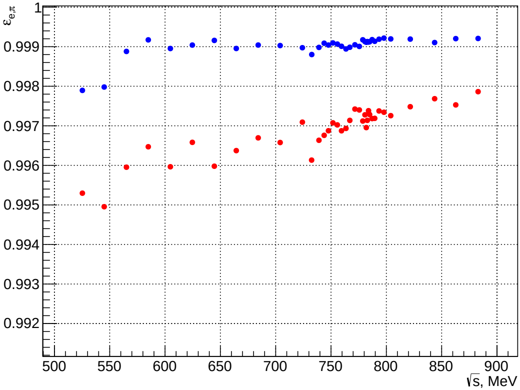

Identification efficiencies for $e^+e^- \to e^+e^-$ and $e^+e^- \to \pi^+\pi^-$ simulated events

ID efficiency correction

$$\delta_x = \frac{\epsilon_x^{exp}}{\epsilon_x^{mc}}$$

$x = e(\pi)$, ϵ_x^{exp} and ϵ_x^{mc} are identification efficiencies for experimental and simulated pseudoevents respectively. The δ_e does not depend on energy, and its average value is 1.0006 ± 0.0001

$$\delta_\pi(\sqrt{s}) = a\left(\sqrt{(\sqrt{s}-b)^2+10} - (\sqrt{s}-b)\right) + c$$

$\delta_\pi = 0.9990 \pm 0.0002$ at the energy region $\sqrt{s} > 0.65$ GeV and below δ_π changes upto 0.9950 ± 0.0006 at $\sqrt{s} = 0.52$ GeV

ID efficiency correction

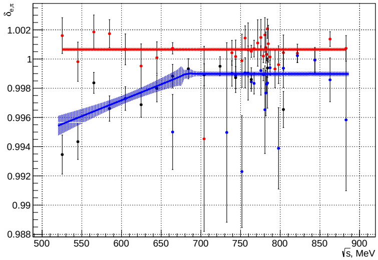

Correction coefficients for ID efficiencies of the $e^+e^- \to e^+e^-$ and $e^+e^- \to \pi^+\pi^-$ events. δ_π obtained using pseudo $\pi\pi$ events constructed from $e^+e^- \to \pi^+\pi^-$ and $e^+e^- \to \omega, \phi \to \pi^+\pi^-\pi^0$ events. Lines are the fit results.

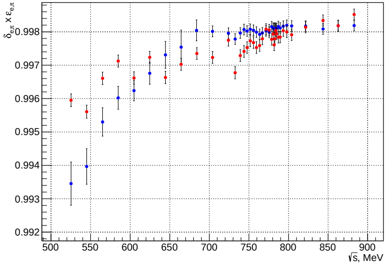

Corrected ID efficiencies for the $e^+e^- \to e^+e^-$ and $e^+e^- \to \pi^+\pi^-$ events

JINST T01002 (2017)

Contribution to the cross section uncertainty

Error	δ_e, %	δ_π at $\sqrt{s} > 0.65$ GeV, %	δ_π at $\sqrt{s} < 0.65$ GeV, %
σ_{stat}	0.01	0.02	0.02 – 0.06
σ_{ID}	0.02	0.01	0.02
σ_{bkg}	0.02	0.02	–
σ_{tot}	0.03	0.03	0.03 – 0.06

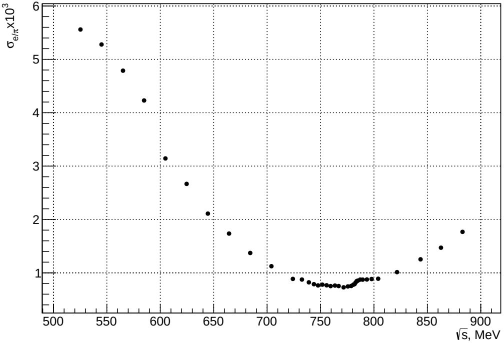

Contribution of the ID efficiencies to the relative error of $e^+e^- \to \pi^+\pi^-$ cross section is **less than 0.2%** for the most energy points

$E_{1,2} > 40$ MeV efficiency

The pseudo–$\pi\pi$ events are used to check the validity of efficiency for the $E_{1,2} > 40$ MeV cut, derived from the simulation

Obtained average correction is equal to **0.992**. The maximum difference between corrections derived from the different types of pseudo-events is **0.5%**

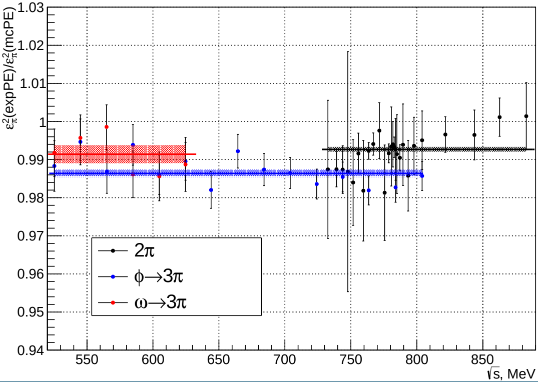

In order to study the differences between simulation and experimental data at each energy point, an efficiency correction is introduced:

$$R_i(x) = \frac{\epsilon_i^{exp}(x)}{\epsilon_i^{mc}(x)} \quad \epsilon_i^{exp} = \frac{N_i(x \in [A_x; B_x])}{N_i(x \in [C_x; D_x])} \quad \epsilon_i^{mc} = \frac{M_i(x \in [A_x; B_x])}{M_i(x \in [C_x; D_x])}$$

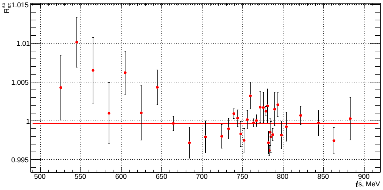

$e^+e^- \to \pi^+\pi^-$

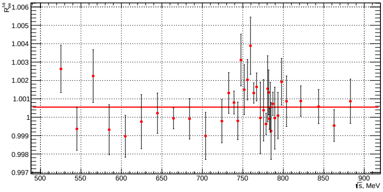

$e^+e^- \to e^+e^-$

Efficiency of the $|\Delta\phi| < 4^\circ$ and $|\Delta\theta| < 12^\circ$ cuts

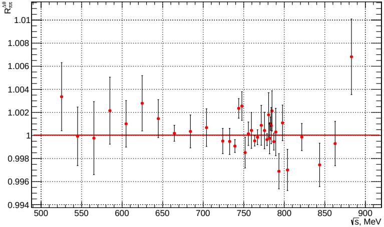

$e^+e^- \to \pi^+\pi^-$

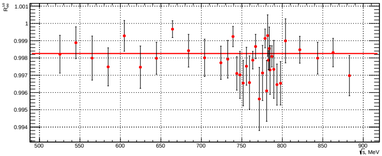

$e^+e^- \to e^+e^-$

The average values of $\delta_{\Delta\phi} = R_{\pi\pi}(\Delta\phi)/R_{ee}(\Delta\phi)$ and $\delta_{\Delta\theta} = R_{\pi\pi}(\Delta\theta)/R_{ee}(\Delta\theta)$ differ from 1 by 0.1 % and 0.2 %, respectively

The overall contribution to the systematic uncertainty from the conditions on the $\Delta\phi$ and $\Delta\theta$ is equal to $0.001 \oplus 0.002 = 0.002$

Efficiency of the $50^\circ < \theta_0 < 130^\circ$ cut

$$R_i(z) = \frac{\varepsilon_i^{exp}(z)}{\varepsilon_i^{mc}(z)} \quad \varepsilon_i^{exp}(z) = \frac{N_i(\theta_0 \in [x; 180^\circ - z])}{N_i(\theta_0 \in [50^\circ; 130^\circ])} \quad \varepsilon_i^{mc}(z) = \frac{M_i(\theta_0 \in [x; 180^\circ - z])}{M_i(\theta_0 \in [50^\circ; 130^\circ])}$$

The statistically significant deviation of $\delta_{\theta_0} = R_{\pi\pi}/R_{ee}$ from unity does not exceed 0.5 %

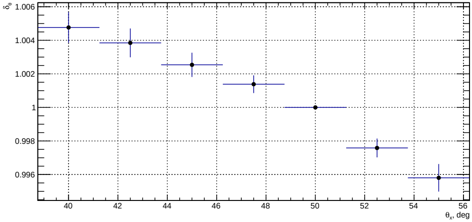

Track reconstruction efficiency

Probability of the π (e) track loss due reconstruction inefficiency is estimated from the $R_{\pi\pi}$ (R_{ee}):

the ratio of the number of events with one track, but the total number of particles > 1 and loosen $\Delta\phi$ and $\Delta\theta$ cuts, to the number of events with two or more tracks

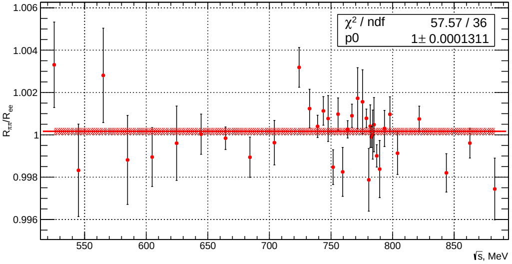

The ratio of $R_{\pi\pi}$ to R_{ee} is taken as a correction to the measured cross section

It does not show a significant deviation from unity

Muon system veto efficiency

$$\delta_{veto} = \frac{\sigma_{\pi\pi}((\phi_1+\phi_2-180^\circ)/2 > 166^\circ or < 14^\circ; veto \geq 0)}{\sigma_{\pi\pi}((\phi_1+\phi_2-180^\circ)/2 > 166^\circ or < 14^\circ; veto = 0)}$$

In case of the *veto* ≥ 0 selection the certain number of the **residual cosmic background** events, derived from the fit of the $(z0_1 + z0_2)/2$ with a sum of uniform and normal distributions, is **subtracted** from the total number of the $e^+e^- \to \pi^+\pi^-$ events

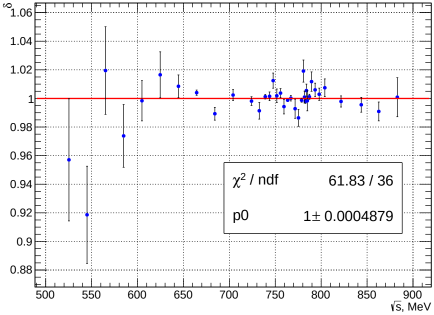

δ_{veto} shows no significant energy dependence

Averaged value is applied and it is consistent with 1

Systematics

The main sources of systematic uncertainty

- $\Delta\theta$, $\Delta\phi$, θ_0 cuts: $0.001 \oplus 0.002 \oplus 0.005 = 0.55\%$
- $E_{1,2} > 40$ MeV condition: 0.5 %
- e/π–separation for the $\sqrt{s} \leq 600$ MeV: 0.3 – 0.5%
- muon subtraction for the $\sqrt{s} \leq 600$ MeV: 0.3 – 0.7%

Additional sources of systematic uncertainty

- 0.2 % is taken as a systematic error from modeling of the pion loss due to nuclear interaction
- Contributions from the $N_{cha} \geq 2$ and $veto = 0$ cuts are considered to be negligible
- Calculation of the radiative correction gives 0.2 %
- 0.1 % from variation of the trigger cuts

Systematics

Source	$\sqrt{s} > 600$ MeV	$\sqrt{s} \leq 600$ MeV
ID e/π	0.1-0.2	0.3-0.5
μ	0.0-0.2	0.3-0.7
$\Delta\theta$	0.1	
$\Delta\phi$	0.2	
θ_0	0.5	
$E_{1,2}$	0.5	
rad	0.2	
trig	0.1	
nucl	0.2	
total	0.8	0.9-1.2

Calculating $e^+e^- \to \pi^+\pi^-$ cross section

$$N_a = L(\sigma_{\pi\pi}\varepsilon^a_{\pi\pi} + \sigma_{\mu\mu}\varepsilon^a_{\mu\mu} + \sigma_{ee}\varepsilon^a_{ee}) + N^a_{nc}$$

a $=$ 1,2 correspond to the $R_{e/\pi} \in [0,1]$ and $R_{e/\pi} \in [-1,0]$ respectively; σ_{jj} and ε^a_{jj}, with jj $= \pi^+\pi^-, \mu^+\mu^-, e^+e^-$ in the final state; N^a_{nc} is the number of non-collinear and cosmic background events; L is the IL collected at s_i.

From these equations $e^+e^- \to \pi^+\pi^-$ cross section and L can be deduced:

$$L(s_i) = \frac{(N_2 - N^2_{nc})\varepsilon^1_{\pi\pi} - (N_1 - N^1_{nc})\varepsilon^2_{\pi\pi}}{\sigma_{ee}(\varepsilon^2_{ee}\varepsilon^1_{\pi\pi} - \varepsilon^1_{ee}\varepsilon^2_{\pi\pi}) + \sigma_{\mu\mu}(\varepsilon^2_{\mu\mu}\varepsilon^1_{\pi\pi} - \varepsilon^1_{\mu\mu}\varepsilon^2_{\pi\pi})}$$

$$\sigma_{\pi\pi}(s_i) = \frac{N_1 - N^1_{nc} - L(s_i)\sigma_{\mu\mu}\varepsilon^1_{\mu\mu}(s_i) - L(s_i)\sigma_{ee}\varepsilon^1_{ee}}{L(s_i)\varepsilon^1_{\pi\pi}}$$

Born cross section

$$\sigma^0_{\pi\pi}(s_i) = \frac{\sigma_{\pi\pi}(s_i)}{1+\delta_{rad}(s_i)}$$

$1+\delta_{rad}(s_i)$ is a **radiative correction**, that accounts for radiation from the initial and final states, calculated using the **MCGPJ** code.

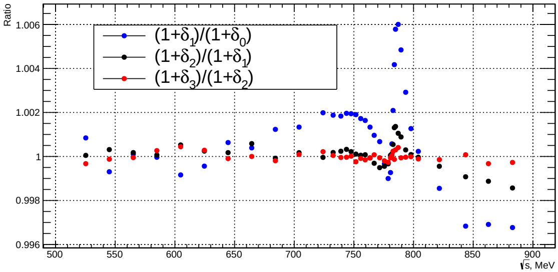

JHEP **9710**, 006 (1997)

$\delta_{rad}(s_i)$ has to be calculated **iteratively**, by fitting measured cross sections with a model from the MCGPJ

Fit model

$$\sigma_{\pi\pi}(s) = \frac{2}{3}\frac{\alpha^2}{s^{5/2}} P_{\pi\pi}(s)|A_{\pi\pi}(s)|^2$$

$$P_{\pi\pi}(s) = q_\pi^3(s), \quad q_\pi(s) = \frac{1}{2}\sqrt{s - 4m_\pi^2}$$

$$|A_{\pi\pi}(s)|^2 = \left| \sqrt{\frac{3}{2}}\frac{1}{\alpha} \sum_{V=\rho,\omega,\rho'} \frac{\Gamma_V m_V^3 \sqrt{m_V \sigma(V \to \pi^+\pi^-)}}{D_V(s)} \frac{e^{i\phi_{\rho V}}}{\sqrt{q_\pi^3(m_V)}} \right|^2$$

$$D_V(s) = m_V^2 - s - i\sqrt{s}\Gamma_V(s), \quad \Gamma_V(s) = \sum_f \Gamma(V \to f, s)$$

$$\Gamma_\omega(s) = \frac{m_\omega^2}{s}\frac{q_\pi^3(s)}{q_\pi^3(m_\omega)}\Gamma_\omega B_{\omega\to\pi^+\pi^-} + \frac{q_{\pi\gamma}^3(s)}{q_{\pi\gamma}^3(m_\omega)}\Gamma_\omega B_{\omega\to\pi^0\gamma} + \frac{W_{\rho\pi}(s)}{W_{\rho\pi}(m_\omega)}\Gamma_\omega B_{\omega\to 3\pi}$$

$$\Gamma_V(s) = \frac{m_V^2}{s}\frac{q_\pi^3(s)}{q_\pi^3(m_V)}\Gamma_V \quad (V = \rho, \rho')$$

Fit results

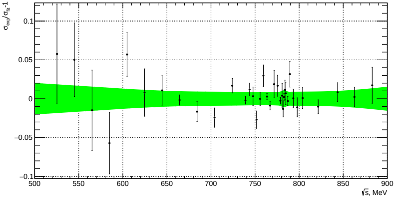

The **relative difference** between the $e^+e^- \to \pi^+\pi^-$ cross section, measured by SND and fit of the SND experimental data. The **green bar** depicts **systematic** and **statistical** errors of the SND fit, folded quadratically.

Cross section values in the $\sqrt{s}$ =352.02, 375.85 and 389.36 MeV energy points shows **non-statistical** deviation from the fit

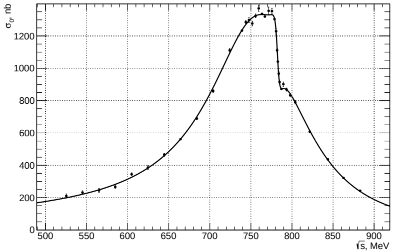

Fit results

parameter	SND VEPP-2000	SND VEPP-2M
m_ρ, MeV	$775.4 \pm 0.5 \pm 0.4$	$774.6 \pm 0.4 \pm 0.5$
Γ_ρ, MeV	$145.8 \pm 0.7 \pm 1$	$146.1 \pm 0.8 \pm 1.5$
$\sigma(\rho \to \pi^+\pi^-)$, nb	$1189.25 \pm 4.6 \pm 9.5$	$1193 \pm 7 \pm 16$
$\sigma(\omega \to \pi^+\pi^-)$, nb	$31.3 \pm 1.3 \pm 0.3$	$29.3 \pm 1.4 \pm 1.0$
$\phi_{\rho\omega}$, deg.	$110.9 \pm 1.5 \pm 0.7$	$113.7 \pm 1.3 \pm 2.0$
$\sigma(\rho' \to \pi^+\pi^-)$, nb	2.3 ± 0.6	1.8 ± 0.2
χ^2/ndf	43/30	–

parameters	SND VEPP-2000	SND VEPP-2M
$B_{\rho\to e^+e^-} \times B_{\rho\to\pi^+\pi^-}$	$(4.888 \pm 0.02 \pm 0.04) \times 10^{-5}$	$(4.876 \pm 0.02 \pm 0.06) \times 10^{-5}$
$B_{\omega\to e^+e^-} \times B_{\omega\to\pi^+\pi^-}$	$(1.312 \pm 0.06 \pm 0.01) \times 10^{-6}$	$(1.225 \pm 0.06 \pm 0.04) \times 10^{-6}$

Fit results

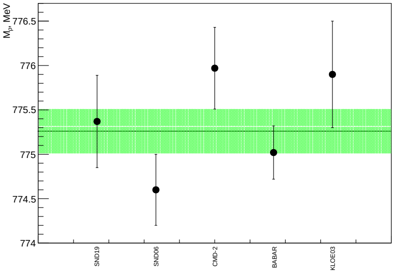
M_ρ, MeV
776.5
776
775.5
775
774.5
774
SND19
SND06
CMD-2
BABAR
KLOE03

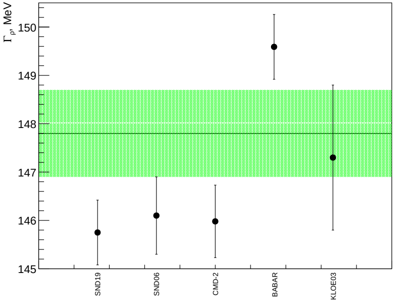
Γ_ρ, MeV
150
149
148
147
146
145
SND19
SND06
CMD-2
BABAR
KLOE03

Calculating bare $e^+e^- \to \pi^+\pi^-$ cross section

$$\sigma^{bare}_{\pi\pi}(s) = \sigma^0_{\pi\pi}(s) \times |1 - \Pi(s)|^2 \times (1 + \frac{\alpha}{\pi} a(s))$$

$$a(s) = \frac{1+\beta^2}{\beta}\left[4Li_2\left(\frac{1-\beta}{1+\beta}\right) + 2Li_2\left(-\frac{1-\beta}{1+\beta}\right) - 3\ln\frac{2}{1+\beta}\ln\frac{1+\beta}{1-\beta} - 2\ln\beta\ln\frac{1+\beta}{1-\beta}\right] - 3\ln\frac{4}{1-\beta^2} - 4\ln\beta + \frac{1}{\beta^3}\left[\frac{5}{4}(1+\beta^2)^2 - 2\right] \times \ln\frac{1+\beta}{1-\beta} + \frac{3}{2}\frac{1+\beta^2}{\beta^2}.$$

$$Li_2(x) = -\int_0^x dt\,\ln(1-t)/t, \quad \beta = \sqrt{1 - \frac{4m_\pi^2}{s}}$$

$$\mathbf{a}_\mu(\pi\pi, s_{min} \leq \sqrt{s} \leq s_{max}) = \left(\frac{\alpha m_\mu}{3\pi}\right)^2 \int_{s_{min}}^{s_{max}} \frac{R(s)K(s)}{s^2} ds$$

$K(s)$ is a known kernel (J. Phys. G **38**, 085003 2011) and

$$R(s) = \frac{\sigma_{\pi\pi}^{bare}}{\sigma(e^+e^- \to \mu^+\mu^-)}, \quad \sigma(e^+e^- \to \mu^+\mu^-) = \frac{4\pi\alpha^2}{3s}$$

Trapezoid integration allows to compute $\mathbf{a}_\mu$ using measured cross sections

	SND VEPP-2000	SND VEPP-2M	BaBar
$a_\mu(\pi\pi) \times 10^{10}$	$410.88 \pm 1.02 \pm 3.75$	$408.88 \pm 1.30 \pm 5.31$	$414.93 \pm 1.02 \pm 2.07$

The relative difference between the $e^+e^- \to \pi^+\pi^-$ cross section, measured by BABAR and fit of the SND experimental data

- $\sigma_{sys} \oplus \sigma_{stat}$ errors are shown for the BABAR data
- The green bar depicts systematic and statistical errors of the SND fit, folded quadratically

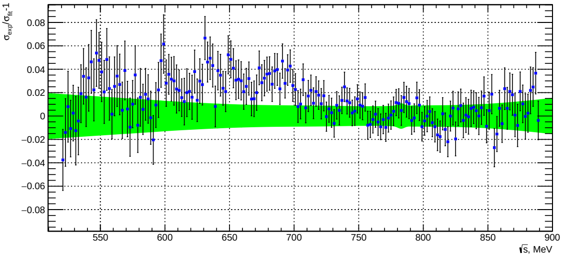

Phys. Rev. 2012.Vol. 86D. 3,032013

The relative difference between the $e^+e^- \to \pi^+\pi^-$ cross section, measured by KLOE and fit of the SND experimental data

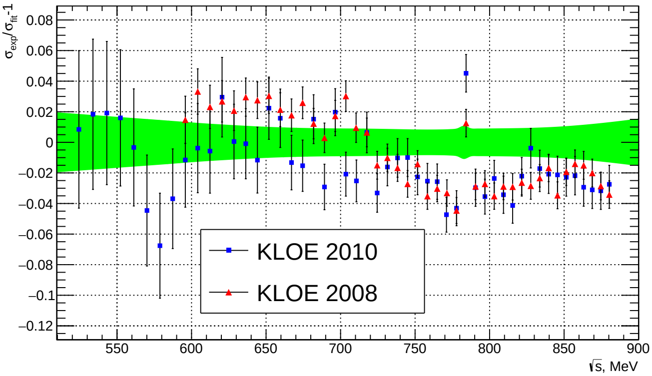

Phys. Lett. 2009. Vol. 670B 4-5, P.285-291

Phys. Lett. 2011. Vol. 700B 2. P.102-110

The relative difference between the $e^+e^- \to \pi^+\pi^-$ cross section, measured in experiments at VEPP-2M and fit of the SND experimental data

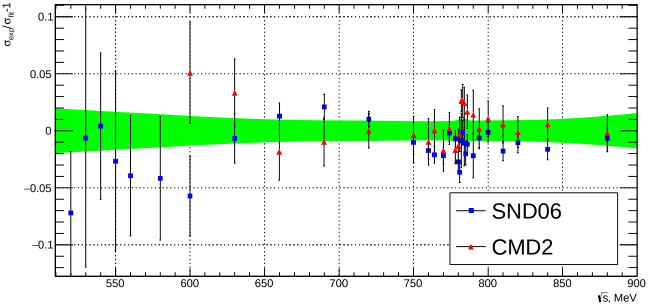

JETP (2006) vol. 103, N3, pp 380-384.
Phys. Lett. 2007 Vol.648B 5. P.28-38

$e^+e^- \to \pi^+\pi^-$ summary

- The difference between the value of $a_\mu(\pi\pi, 525\text{MeV} \leq \sqrt{s} \leq 883\text{MeV})$ obtained from the SND data, and ones derived from the previous measurements $< 1\sigma$
- The parameters of the ρ and ω mesons in this analysis are consistent with ones obtained by SND in experiments at VEPP-2M
- Comparison with VEPP-2M results indicates no significant contradictions in the whole energy spectrum
- In the $0.6 \geq \sqrt{s} \leq$0.7 GeV energy range there is a 3% discrepancy between the SND and BABAR data, but for the rest of the spectrum SND data is in agreement with the BABAR results
- There is 1–3 % deviation between KLOE and SND data for $\sqrt{s} \geq$0.7 GeV

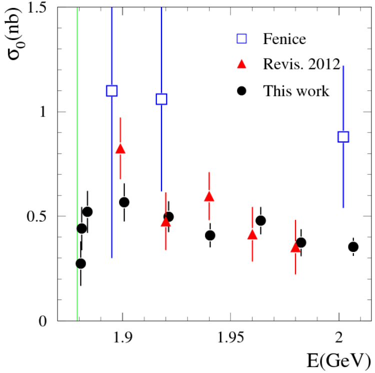

Cross Section measurement

- The new measurement is based on the 2017 dataset and uses a different method. The calorimeter-trigger-time distribution is analyzed.
- Our new result is lower than the previous SND measurement. The reasons are underestimated beam background and incorrect MC simulation.
- The systematic uncertainty on the cross section is estimated to be about 20%, mainly due to MC simulation.

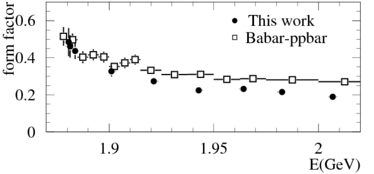

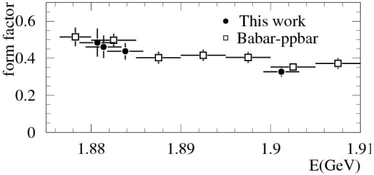

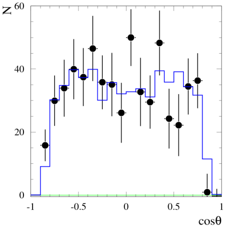

Formfactor

- The cross section depends on two form factors.
- From the measured cross section we determine the effective form factor
- Near threshold the proton and neutron effective form factors are close to each other. The neutron form factor become lower than the proton one with increase the energy.
- The ratio of the form factors can be determined from the analysis of the $cos(\theta)$ distribution

G_E

- The $cos(\theta)$ distribution is well described by $1 + cos(\theta)^2$, i.e. G_E=0.
- For proton $|G_E/G_M| \approx 1.5$ in this energy region.

$e^+e^- \to \pi^+\pi^-\pi^0\eta$

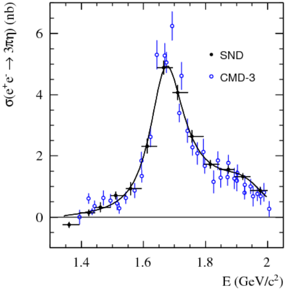

The total $e^+e^- \to \pi^+\pi^-\pi^0\eta$ cross section measured by SND is, in general, consistent with the CMD-3 result. The $\approx 15\%$ difference in the cross section maximum is within the systematic uncertainties, which are 7% for SND and 11% for CMD-3.

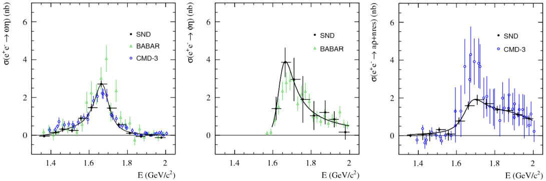

Exclusive chanels

- The obtained $\omega\eta$ cross section agrees with the CMD-3 measurement. Both the SND and CMD-3 results lie below the BABAR data.
- The SND and BABAR $\phi\eta$ easurements are in reasonable agreement.
- The significant difference between the SND and CMD-3 measurements is observed for the $a_0\rho$+strucrureless final state.

$e^+e^- \to \eta\pi^0\gamma$

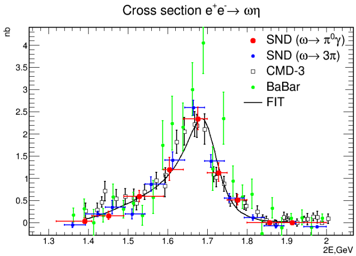

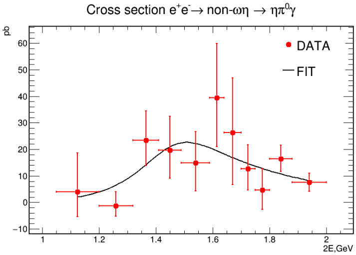

$e^+e^- \to \omega\eta \to \eta\pi^0\gamma$

The measured $e^+e^- \to \omega\eta$ cross section is in good agreement with the SND and CMD-3 measurements in the $\omega \to 3\pi$ decay mode.

- The radiative $e^+e^- \to \eta\pi^0\gamma$ process was studied previously only in the $\phi(1020)$ region.
- We perform the **first measurement** in the energy range 1.05-2.00 GeV.
- The value of the cross section is about 15-20 pb in the region 1.4-1.9 GeV.

$e^+e^- \to \eta$ and $e^+e^- \to f_1(1285)$

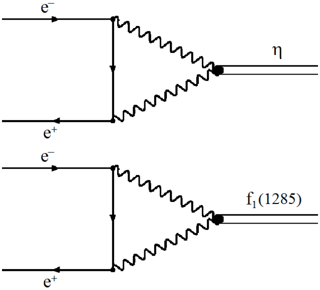

$e^+e^- \to \eta$

- The 650 nb^{-1} data sample was recorded in 2018 at $\sqrt{s} = m_\eta$.
- The decay mode $\eta \to 3\pi^0$ is used, in which the single photon annihilation background is absent.
- Zero signal events have been selected.
- The upper limit $B(\eta \to e^+e^-) < 7 \times 10^{-7}$ at 90% CL has been set.

$e^+e^- \to f_1(1285)$

- About 4 pb^{-1} of data were collected in the resonance maximum.
- The $f_1(1285) \to \pi^0\pi^0\eta \to 6\gamma$ decay mode is used.
- The main background sources are $e^+e^- \to \omega\pi^0 \to \pi^0\pi^0\gamma$, $e^+e^- \to \eta\gamma$ and $e^+e^- \to \pi^0\pi^0\omega$.
- After applying the selection criteria, two events have been observed at the peak.
- These two events correspond to $B(f_1(1285) \to e^+e^-) = 6.1^{+3.6}_{-2.6} \times 10^{-9}$

Conclusion

- The $e^+e^- \to \pi^+\pi^-$ cross section is measured with systematic uncertainty better then 1%
- The accuracy of $e^+e^- \to n\bar{n}$ measurement is significantly improved
- The $e^+e^- \to \pi^+\pi^-\pi^0\eta$ cross section has been measured
- Rare radiative process $e^+e^- \to \eta\pi^0\gamma$ have been measured for the first time in the energy range 1.05-2.00 GeV
- Search for production of C-even resonances, η and $f_1(1285)$, in e^+e^- annihilation is performed. The first indication of the process $e^+e^- \to f_1(1285)$ is obtained

$\sqrt{s}$, MeV	σ, nb	σ_0, nb	$\lvert F(s)\rvert^2$	σ_{bare}, nb
525.3	203.3±12.3	210.3±12.7	4.4±0.3	209.6±12.7
545	223.5±10.1	231.7±10.4	5±0.2	231.2±10.4
565.1	235±12.3	244.4±12.8	5.5±0.3	243.9±12.8
584.9	254.7±10.7	265.8±11.2	6.2±0.3	265.5±11.1
604.8	328.5±8.7	344.4±9.1	8.3±0.2	344.5±9.1
624.7	366.5±11.1	386.2±11.7	9.7±0.3	386.7±11.7
644.6	438.2±8.2	464.5±8.7	12.1±0.2	465.8±8.8
664.4	526.4±3.5	561.5±3.7	15.3±0.1	564±3.7
684.2	642.1±8.4	689.4±9	19.5±0.3	693.1±9.1
704	797.3±10.2	859.8±11	25.4±0.3	864.6±11.1
724.1	1029.3±9.5	1111.2±10.3	34.2±0.3	1115.2±10.3
739.1	1146.5±5.6	1233.5±6	39.1±0.2	1233.7±6
743.8	1197.9±9.8	1285.8±10.5	41.1±0.3	1284.5±10.5
747.7	1212.1±14.4	1298.2±15.4	41.9±0.5	1295.3±15.4
751.7	1195.5±13.7	1277.2±14.6	41.5±0.5	1272.4±14.6
755.7	1243.9±10.8	1324.7±11.5	43.4±0.4	1318.2±11.4
759.5	1291.2±17.3	1370.7±18.4	45.3±0.6	1363.1±18.2

$\sqrt{s}$, MeV	σ, nb	σ_0, nb	$\lvert F(s)\rvert^2$	σ_{bare}, nb
763.5	1263.7±5	1336.7±5.2	44.5±0.2	1328.9±5.2
767	1251.9±6.9	1320.2±7.3	44.3±0.2	1312.9±7.2
771.6	1289.8±22.2	1355.6±23.3	45.9±0.8	1350.9±23.2
775.6	1291.3±17.2	1353.9±18	46.2±0.6	1353.5±18
778.7	1251.6±5.3	1304.3±5.5	44.8±0.2	1300.7±5.5
780.7	1198.1±18.4	1229±18.9	42.4±0.7	1212.9±18.6
781.9	1105.1±11.2	1111.4±11.2	38.4±0.4	1081.6±10.9
782.8	1056.2±4.8	1041.3±4.7	36±0.2	1001.4±4.5
783.9	1000.8±11.6	967.2±11.2	33.5±0.4	917.7±10.6
784.9	957.3±12.8	915.3±12.2	31.8±0.4	862.6±11.5
787.1	911.3±5.1	872.1±4.8	30.4±0.2	818.7±4.5
789.5	933±14.1	901.8±13.6	31.6±0.5	849.8±12.8
793.4	891.7±10	868.5±9.7	30.7±0.3	823.3±9.2
797.8	856±10.1	833±9.8	29.7±0.4	792.8±9.3
804	818.3±10.4	789.9±10.1	28.5±0.4	754.1±9.6
821.6	654.4±5.6	608.4±5.2	22.7±0.2	582.6±5
843.6	496±5.8	436.9±5.1	17±0.2	419.5±4.9
862.7	383.4±4.6	322±3.9	13±0.2	309.8±3.8
882.9	303.2±6.7	242.3±5.3	10.2±0.2	233.7±5.1